



THE UNIVERSITY *of* EDINBURGH

Edinburgh Research Explorer

Oscillatory rarefied gas flow inside rectangular cavities

Citation for published version:

Wu, L, Reese, JM & Zhang, Y 2014, 'Oscillatory rarefied gas flow inside rectangular cavities', *Journal of Fluid Mechanics*, vol. 748, pp. 350-367. <https://doi.org/10.1017/jfm.2014.183>

Digital Object Identifier (DOI):

[10.1017/jfm.2014.183](https://doi.org/10.1017/jfm.2014.183)

Link:

[Link to publication record in Edinburgh Research Explorer](#)

Document Version:

Publisher's PDF, also known as Version of record

Published In:

Journal of Fluid Mechanics

General rights

Copyright for the publications made accessible via the Edinburgh Research Explorer is retained by the author(s) and / or other copyright owners and it is a condition of accessing these publications that users recognise and abide by the legal requirements associated with these rights.

Take down policy

The University of Edinburgh has made every reasonable effort to ensure that Edinburgh Research Explorer content complies with UK legislation. If you believe that the public display of this file breaches copyright please contact openaccess@ed.ac.uk providing details, and we will remove access to the work immediately and investigate your claim.



Oscillatory rarefied gas flow inside rectangular cavities

Lei Wu¹, Jason M. Reese² and Yonghao Zhang^{1,†}

¹James Weir Fluids Laboratory, Department of Mechanical and Aerospace Engineering, University of Strathclyde, Glasgow G1 1XJ, UK

²School of Engineering, University of Edinburgh, Edinburgh EH9 3JL, UK

(Received 17 December 2013; revised 19 February 2014; accepted 31 March 2014)

Two-dimensional oscillatory lid-driven cavity flow of a rarefied gas at arbitrary oscillation frequency is investigated using the linearized Boltzmann equation. An analytical solution at high oscillation frequencies is obtained, and detailed numerical results for a wide range of gas rarefaction are presented. The influence of both the aspect ratio of the cavity and the oscillating frequency on the damping force exerted on the moving lid is studied. Surprisingly, it is found that, over a certain frequency range, the damping is smaller than that in an oscillatory Couette flow. This reduction in damping is due to the anti-resonance of the rarefied gas. A scaling law between the anti-resonant frequency and the aspect ratio is established, which would enable the control of the damping through choosing an appropriate cavity geometry.

Key words: micro-/nano-fluid dynamics, rarefied gas flow

1. Introduction

The study of rarefied gas flows at the micro- (or nano-) scale is important for a broad range of industrial applications, and has attracted particular attention due to the rapid development of micro-electromechanical systems (MEMS) (Karniadakis, Beskok & Aluru 2005). An important research topic is to investigate the damping force that any oscillatory parts of a MEMS device are subject to, which has applications in inertial sensing and acoustic transduction. The normal pressure and shear force from the ambient gas damp the vibrating parts. Because of the small length scale of MEMS devices, and sometimes the high frequency of oscillation, the damping force should be calculated based on a kinetic theory that recognizes the rarefied nature of the flow, instead of models (such as the Navier–Stokes equations) derived from the continuum-fluid hypothesis.

In the past decade, in order to investigate the damping due to the normal pressure, the propagation of sound waves (Hadjiconstantinou 2002; Sharipov & Kalempa 2008*a*; Kalempa & Sharipov 2009; Gu & Emerson 2011; Struchtrup 2011; Desvillettes & Lorenzani 2012; Kalempa & Sharipov 2012) between two parallel plates or in a semi-infinite space has been extensively studied; to investigate the damping caused by the shear force, oscillatory Couette flows both in planar (Park, Bahukudumbi

† Email address for correspondence: yonghao.zhang@strath.ac.uk

& Beskok 2004; Tang *et al.* 2008; Sharipov & Kalempa 2008*b*; Doi 2009; Taheri *et al.* 2009; Yap & Sader 2012) and cylindrical geometries (Emerson *et al.* 2007; Shi & Sader 2010; Gospodinov, Roussinov & Stefan 2012) have been studied. For these investigations the adopted methods have included the direct simulation Monte Carlo (DSMC) method (Bird 1994), the discrete velocity method for the linearized Bhatnagar–Gross–Krook (BGK), ellipsoidal statistical BGK, and Shakhov kinetic model equations (Bhatnagar, Gross & Krook 1954; Holway 1966; Shakhov 1968), the numerical kernel method for the linearized Boltzmann equation of hard-sphere gases (Doi 2009), the regularized 13- and 26-moment equations (Struchtrup 2005; Gu & Emerson 2011), and the lattice Boltzmann method (Tang *et al.* 2008; Meng & Zhang 2011).

However, the above-mentioned studies are all for one-dimensional (1D) or quasi-one-dimensional (cylindrical) geometries. This implicitly assumes that dimensions in other directions are large enough so that the flow in the direction of interest is not affected. In this paper we take a step further and study the rarefied gas flow inside a two-dimensional (2D) rectangular cavity driven by the periodic oscillation of the top lid. Specifically, we investigate the influence of both the aspect ratio of the cavity and the oscillating frequency of the lid on flow properties such as the average amplitudes of shear stress and velocity at the lid. This research sheds new light on controlling the damping force associated with an oscillating component by choosing an appropriate geometry of the MEMS device.

We use the Boltzmann equation to describe the rarefied gas dynamics, which can be linearized due to the fact that the velocity of the oscillating component is far smaller than the most probable molecular velocity, so that the deviation from the global equilibrium state is small. Therefore, instead of using the DSMC method that is subject to intrinsic noise and requires a time step smaller than both the molecular mean collision time and the characteristic oscillation time, the oscillatory flow is solved by a deterministic numerical method that is free of noise and from which, more importantly, time-dependence can be eliminated (Sharipov & Kalempa 2008*a,b*). We approximate the linearized Boltzmann collision operator by the fast spectral method (Wu, Reese & Zhang 2014), and solve the time-independent linearized Boltzmann equation in an iterative manner. The numerical efficiency of this approach is much better than the DSMC method, especially for high-frequency lid oscillations.

2. Formulation of the problem

We consider a rarefied gas flow inside a 2D cavity of rectangular cross-section, driven by a lid at $y=H$ that oscillates harmonically in the x direction with frequency Ω ; see figure 1. The velocity U_w of the lid depends on time t through

$$U_w = \text{Re}[U_0 \exp(i\Omega t)], \quad (2.1)$$

where i is the imaginary unit, Re denotes the real part of a complex expression, and U_0 is the velocity amplitude of the oscillating lid. The other three cavity walls at $x=0$, $y=0$, and $x=L$ are fixed. All four walls are isothermal with a common temperature T_0 , and the diffuse boundary condition is employed.

The induced oscillatory rarefied flows inside the cavity are characterized by the aspect ratio of the cavity

$$A = \frac{L}{H}, \quad (2.2)$$

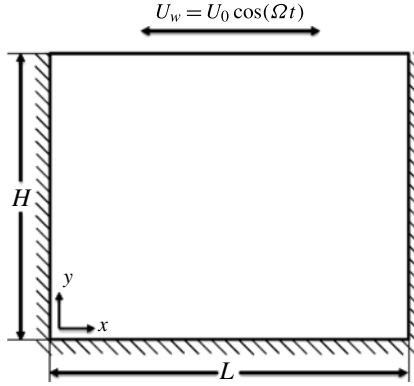


FIGURE 1. Configuration for the oscillatory lid-driven cavity flow of a rarefied gas.

the Knudsen number

$$Kn = \frac{\mu}{n_0 H} \sqrt{\frac{\pi}{2mk_B T_0}}, \quad (2.3)$$

and the Strouhal number

$$St = \frac{\Omega H}{v_m}, \quad (2.4)$$

where μ is the gas shear viscosity at temperature T_0 , n_0 is the number density of the gas at equilibrium, k_B is the Boltzmann constant, m is the molecular mass, and $v_m = \sqrt{2k_B T_0/m}$ is the most probable molecular velocity. Note that the Strouhal number is related to the Stokes number (or the Womersley number) β through $St = \beta^2 Kn / \sqrt{\pi}$ (Park *et al.* 2004).

The induced flow is also affected by the type of intermolecular interactions. However, in our numerical simulations we find that the difference in flow properties between hard-sphere and Maxwell gases is less than 3%: for instance, for $Kn = 0.1$, $A = 1$, and $St = 4$, relative differences in the average amplitudes of the shear stress and the horizontal gas velocity at the oscillating lid are 0.6%, and 1.9%, respectively. The relative difference between a hard-sphere gas and gases with a viscosity index between 0.5 and 1 is even smaller. Therefore, we only consider a hard-sphere gas. The Boltzmann equation reads (Cercignani 1990)

$$\frac{H}{v_m} \frac{\partial f}{\partial t} + v_x \frac{\partial f}{\partial x'} + v_y \frac{\partial f}{\partial y'} = \frac{5}{64\sqrt{2}Kn} \int_{-\infty}^{\infty} \int_0^{2\pi} \int_0^{\pi} |\mathbf{v} - \mathbf{v}_*| (f'_* f' - f_* f) \sin\theta d\theta d\varphi d\mathbf{v}_*, \quad (2.5)$$

where $(x', y') = (x, y)/H$, the velocity \mathbf{v} is normalized by v_m , and the velocity distribution function (VDF) f is normalized by n_0/v_m^3 ; θ is the deflection angle, φ is the azimuthal angle, \mathbf{v}_* is the velocity of the second molecule in a binary collision, and f'_* and f' are the VDFs after binary collision.

If $U_0 \ll v_m$ and the Reynolds number is small, (2.5) can be linearized. We are interested in the gas flow state when the oscillation has been fully established, so that the time-dependent periodic flow has the same frequency Ω as the oscillating lid. To improve numerical efficiency, we eliminate the time variable by including the explicit time-varying term $\exp(i\Omega t)$ and expressing the VDF as

$$f(t, x', y', \mathbf{v}) = f_{eq}(\mathbf{v}) + \text{Re} \left[\exp(i\Omega t) h(x', y', \mathbf{v}) \right] \frac{U_0}{v_m}, \quad (2.6)$$

where

$$f_{eq}(\mathbf{v}) = \frac{\exp(-|\mathbf{v}|^2)}{\pi^{3/2}} \tag{2.7}$$

is the global equilibrium VDF, and $h(x', y', \mathbf{v})$ is the perturbed VDF. On neglecting terms of order higher than U_0/v_m , we arrive at the linearized Boltzmann equation for $h(x', y', \mathbf{v})$, which is independent of time:

$$[iSt + \nu(v)]h + v_x \frac{\partial h}{\partial x'} + v_y \frac{\partial h}{\partial y'} = \mathcal{L}_g(h), \tag{2.8}$$

where

$$\mathcal{L}_g(h) = \frac{5}{64\sqrt{2}Kn} \int_{-\infty}^{\infty} \int_0^{2\pi} \int_0^{\pi} |\mathbf{v} - \mathbf{v}_*| [2f_{eq}(\mathbf{v}')h(\mathbf{v}'_*) - f_{eq}(\mathbf{v})h(\mathbf{v}_*)] \sin\theta d\theta d\varphi d\mathbf{v}_* \tag{2.9}$$

is the linear gain term and

$$\nu(v) = \frac{5}{64\sqrt{2}Kn} \int_{-\infty}^{\infty} \int_0^{2\pi} \int_0^{\pi} |\mathbf{v} - \mathbf{v}_*| f_{eq}(\mathbf{v}_*) \sin\theta d\theta d\varphi d\mathbf{v}_* \tag{2.10}$$

is the equilibrium collision frequency; both of these can be effectively and accurately calculated by the fast spectral method (Wu *et al.* 2014).

The problem is symmetric, due to the negligible Reynolds number, about the central vertical line at $x' = A/2$; so $h(x', y', v_x, v_y, v_z) = -h(A - x', y', -v_x, v_y, v_z)$. Therefore, only the left half-domain ($x' \in [0, A/2]$, $y' \in [0, 1]$) is calculated. The diffuse boundary conditions at the top, left, and bottom walls read

$$h = \begin{cases} \left(2v_x + 2\sqrt{\pi} \int_{v_y>0} v_y h d\mathbf{v} \right) f_{eq}; & y' = 1, \quad v_y < 0, \\ -2\sqrt{\pi} f_{eq} \int_{v_x<0} v_x h d\mathbf{v}; & x' = 0, \quad v_x > 0, \\ -2\sqrt{\pi} f_{eq} \int_{v_y<0} v_y h d\mathbf{v}; & y' = 0, \quad v_y > 0, \end{cases} \tag{2.11}$$

while at the central vertical line, if the VDF $h(A/2, y', v_x, v_y, v_z)$ is known when $v_x > 0$, we have $h(A/2, y', -v_x, v_y, v_z) = -h(A/2, y', v_x, v_y, v_z)$.

The left spatial half-domain is divided into non-uniform grid points, and the molecular velocity space \mathbf{v} is represented by discrete velocity grids. The spatial derivatives in (2.8) are approximated by a second-order upwind finite-difference, and the resulting algebraic equation for the VDF is solved in an iterative manner. Detailed information about the numerical implementation can be found in Wu *et al.* (2014).

The number density, which is normalized by $n_0 U_0/v_m$, is given by

$$n(x', y', t) = \text{Re} \left[\exp(i\Omega t) \int h d\mathbf{v} \right]. \tag{2.12}$$

The macroscopic flow velocities, which are normalized by the velocity amplitude of the oscillating lid, are given by

$$\left. \begin{aligned} u_x(x', y', t) &= \text{Re} \left[\exp(i\Omega t) \int v_x h d\mathbf{v} \right] = \text{Re} \left[\exp(i\Omega t) U_x \right], \\ u_y(x', y', t) &= \text{Re} \left[\exp(i\Omega t) \int v_y h d\mathbf{v} \right] = \text{Re} \left[\exp(i\Omega t) U_y \right], \end{aligned} \right\} \tag{2.13}$$

and the shear stress, which is normalized by $n_0 k_B T_0 U_0 / v_m$, is given by

$$p_{xy}(x', y', t) = \text{Re} \left[\exp(i\Omega t) \int 2v_x v_y h d\mathbf{v} \right] = \text{Re} \left[\exp(i\Omega t) P_{xy} \right]. \quad (2.14)$$

Other macroscopic quantities such as temperature and heat flux can be expressed in a similar way, but they will not be considered here because of their relative smallness (Naris & Valougeorgis 2005) when compared to the magnitudes of velocity and shear stress.

After having solved the problem in the left spatial half-domain, from the symmetric condition about the central vertical line we can obtain the flow properties in the right spatial half-domain according to the following relations: $n(x', y') = -n(A - x', y')$, $U_x(x', y') = U_x(A - x', y')$, $U_y(x', y') = -U_y(A - x', y')$, and $P_{xy}(x', y') = P_{xy}(A - x', y')$.

3. Results and discussion

Numerical results from the fast spectral method are presented below in the slip, transition, and free-molecular flow regimes. For each Knudsen number, the Strouhal number is varied from zero to the high-frequency oscillation limit. The cavity aspect ratios we investigated are $A = 0.5, 1, \text{ and } 2$, and the average velocity and shear stress at the oscillating lid are compared to those of 1D oscillatory Couette flow (which is a limiting case of a 2D oscillatory lid-driven cavity flow with $A = \infty$).

3.1. Analytical solution at the high-frequency limit

Unlike 1D oscillatory Couette flow, where analytical solutions can be found in the continuum, slip, and free-molecular flow regimes (Park *et al.* 2004) as well as at the high-frequency limit (Sharipov & Kalempa 2008b), an analytical solution for oscillatory lid-driven cavity flow can only be obtained at the high-frequency limit; note that the analytical solution is hard to find even in the continuum flow regime (Duck 1982).

When the lid oscillates at high frequency, i.e. when Ω is much larger than the average molecular collision frequency, binary collisions are negligible (Sharipov & Kalempa 2008b). In this situation, (2.8) becomes:

$$iSt h + v_x \frac{\partial h}{\partial x'} + v_y \frac{\partial h}{\partial y'} = 0. \quad (3.1)$$

Integrating (3.1) with respect to x' and introducing the average VDF

$$g(y', \mathbf{v}) = \frac{\int_0^A h dx'}{A}, \quad (3.2)$$

we have

$$iSt g + v_y \frac{\partial g}{\partial y'} = v_x \frac{h(x'=0) - h(x'=A)}{A}. \quad (3.3)$$

At the high-frequency limit, the term on the right-hand side of (3.3) is negligible. Therefore, we have an ordinary differential equation for g :

$$iSt g + v_y \frac{dg}{dy'} = 0. \quad (3.4)$$

Taking into account symmetry about the central vertical line, from (2.11) we know that the boundary condition for g at $y' = 1$ is $g = 2v_x f_{eq}$ when $v_y < 0$, while that at $y' = 0$ is $g = 0$ when $v_y > 0$. Solving (3.4) then yields:

$$g(y', \mathbf{v}) = \begin{cases} 2v_x f_{eq} \exp\left(-iSt \frac{1-y'}{v_y}\right); & v_y < 0, \\ 0; & v_y > 0. \end{cases} \quad (3.5)$$

Therefore, the average amplitude of the horizontal velocity $\bar{U}_x(y') = \int_0^A U_x dx'/A$ and the average amplitude of the shear stress $\bar{P}_{xy}(y') = \int_0^A P_{xy} dx'/A$ are given by

$$\left. \begin{aligned} \bar{U}_x(y') &= \iiint \int_{-\infty}^{\infty} v_x g(\mathbf{v}, y') dv_x dv_z dv_y = \frac{1}{\sqrt{\pi}} I_0[iSt(1-y')], \\ \bar{P}_{xy}(y') &= \iiint \int_{-\infty}^{\infty} 2v_x v_y g(\mathbf{v}, y') dv_x dv_z dv_y = -\frac{2}{\sqrt{\pi}} I_1[iSt(1-y')], \end{aligned} \right\} \quad (3.6)$$

where $I_m(z) = \int_0^{\infty} c^m \exp(-c^2 - z/c) dc$.

These expressions for average amplitudes of horizontal velocity and shear stress are the same as those given by Sharipov & Kalempa (2008b) for 1D oscillatory Couette flow. Of particular interest are the average amplitudes of the horizontal velocity and shear stress at the oscillating lid, which can be simply given as

$$\left. \begin{aligned} |\bar{U}_x(y=H)| &= \frac{1}{2}, \\ |\bar{P}_{xy}(y=H)| &= \frac{1}{\sqrt{\pi}}. \end{aligned} \right\} \quad (3.7)$$

A lid-driven cavity flow with zero oscillation frequency has previously been studied on the basis of the linearized BGK kinetic equation by Naris & Valougeorgis (2005). For fixed aspect ratio, it was found that the average shear stress at the lid increases with Kn and approaches a constant when $Kn \rightarrow \infty$. In the free-molecular limit, for example, the average shear stress is 0.69 for $A = 1$, which is larger than the limiting value $1/\sqrt{\pi}$ that we obtained above at the high-frequency limit. This indicates that changing the oscillation frequency can reduce the damping force at the oscillating lid. Below, we explain this quantitatively by using our numerical method.

3.2. Slip flow regime

We consider a hard-sphere gas at $Kn = 0.1$. The left spatial half-domain is divided into 26×51 non-uniform cells for $A = 0.5$, and 51×51 non-uniform cells for $A = 1$ and 2, with the cell dimensions near the walls being very small. The three-dimensional molecular velocity space is represented by 32×32 non-uniform grid points in the v_x and v_y directions ($v_x, v_y \in [-4, 4]$), with most of the grid points near $v_x, v_y \sim 0$ to capture the discontinuity in the VDF, and 12 uniform grid points in the v_z direction (due to symmetry, only half the velocity space $v_z \in [0, 6]$ is considered). For $A = 1$ and $St = 4$, when the number of spatial cells is increased from 51×51 to 101×101 , the average amplitudes of the shear stress and horizontal velocity at the oscillating lid only change by 0.2% and 0.6%, respectively.

Figure 2(a-c) presents typical instantaneous density and streamline profiles for $A = 0.5$ during the first half-period of oscillation (since the flow variables in the next half-period are of the same magnitude as in the first half period, but with reversed signs).

At small oscillation frequencies (not shown), the induced gas flow is in-phase with the oscillating lid. The streamlines are closed, except in a very small time interval when the lid velocity reverses. The density variations concentrate in the top left and top right corners and are at a maximum when $\Omega t/\pi$ is an integer.

When the frequency increases to $St=2$, the streamlines are closed in the first quarter of the oscillation period (see figure 2*a*); after $\Omega t = \pi/2$, the streamlines are not closed in a short time interval (for instance, see the figure for $\Omega t = 0.55\pi$). When $\Omega t = 0.7\pi$, a source at $y' \approx 0.8$, $x' = A$ and a sink at $y' \approx 0.8$, $x' = 0$ appear. Furthermore, a vortex emerges near the bottom wall. After that, the streamlines are closed again and the vortex moves towards the lid. As St continues to increase, the time interval in which closed streamlines exist becomes shorter. Meanwhile, the phase lag relative to the oscillating lid grows. For example, as seen in figure 2*b*) where $St = 4$, the maximum density variation is achieved near $\Omega t = 0.4\pi$, where the lid velocity is not a maximum.

When the top lid oscillates at high frequency, the streamlines are not closed anymore in the whole oscillation period, and more and more sources and sinks appear along the two vertical walls; see figure 2*c*) where $St = 30$. Also, the flow has a large phase lag relative to the oscillation of the lid. For instance, at $\Omega t = 0.9\pi$, the flow near the lid still moves from left to right, while the lid has started to move towards the left at $\Omega t = \pi/2$. Furthermore, the magnitudes and spatial regions of the density variations are reduced significantly, when compared to cases at smaller Strouhal numbers such as $St = 2$; see the right-hand plots of figures 2*d*) and 2*e*) for $St = 30$. The flow fields for aspect ratios $A = 1$ and 2 are similar, except that no vortex develops near the bottom wall; see the results for $St = 2$ and $\Omega t = 0.7\pi$ in figure 2*a*).

Figure 3 shows the evolution of the vortex centre during the first half-period of oscillation. If two or more vortices exist, only the one near the oscillatory lid is selected. Since the vortex centre is located along the central vertical line, only its y -location is shown. Let us first examine figure 3*a*) for $A = 0.5$. When $St = 2$, the vortex centre approaches the oscillating lid from $y = 0.85H$ to $0.94H$ monotonically during $0 \leq \Omega t \leq \pi/2$. After the lid velocity reverses, for a short time interval ($\pi/2 < \Omega t < 0.64\pi$) there is no vortex (the typical streamlines in this situation are shown in figure 2*a*) for $St = 2$ and $\Omega t = 0.55\pi$). Then a vortex appears near the bottom wall (see the streamlines in figure 2*a*) for $St = 2$ and $\Omega t = 0.7\pi$) which quickly moves towards the top wall after $\Omega t = 0.79\pi$. As St increases, the time needed to form a vortex increases after the lid velocity reverses. As a consequence, there is no vortex during $\pi/2 < \Omega t \leq \pi$ for $St > 3$. Specifically, no vortex exists during $\pi/2 < \Omega t < 1.14\pi$ and $\pi/2 < \Omega t < 1.38\pi$ for $St = 4$ and $St = 5$, respectively. For $St > 5.5$, there is no vortex during the whole oscillation period. When $A = 1$ or 2, the situation is similar (figure 3*b,c*).

Figure 4 demonstrates how the amplitudes of the velocity and shear stress change with the Strouhal number when $A = 1$. Here, the amplitude of the central horizontal velocity $U_x(x = L/2)$ is defined such that the phase of this velocity at $y = H$ is zero, while for the central vertical velocity $U_y(y = H/2)$ the phase at $x = 0$ is chosen to be zero. For U_x and P_{xy} at $y = H$, the phases at the middle of the oscillating lid are chosen to be zero and π , respectively. For $St \leq 4$, the amplitude of the central horizontal velocity in the region $0.9H < y \leq H$ does not change with St (figure 4*a*). At large values of St , from the top wall to the bottom, the amplitude of the central horizontal velocity rapidly reduces. For the central vertical velocity (figure 4*b*), its magnitude gradually decreases as St increases and finally becomes zero. However,

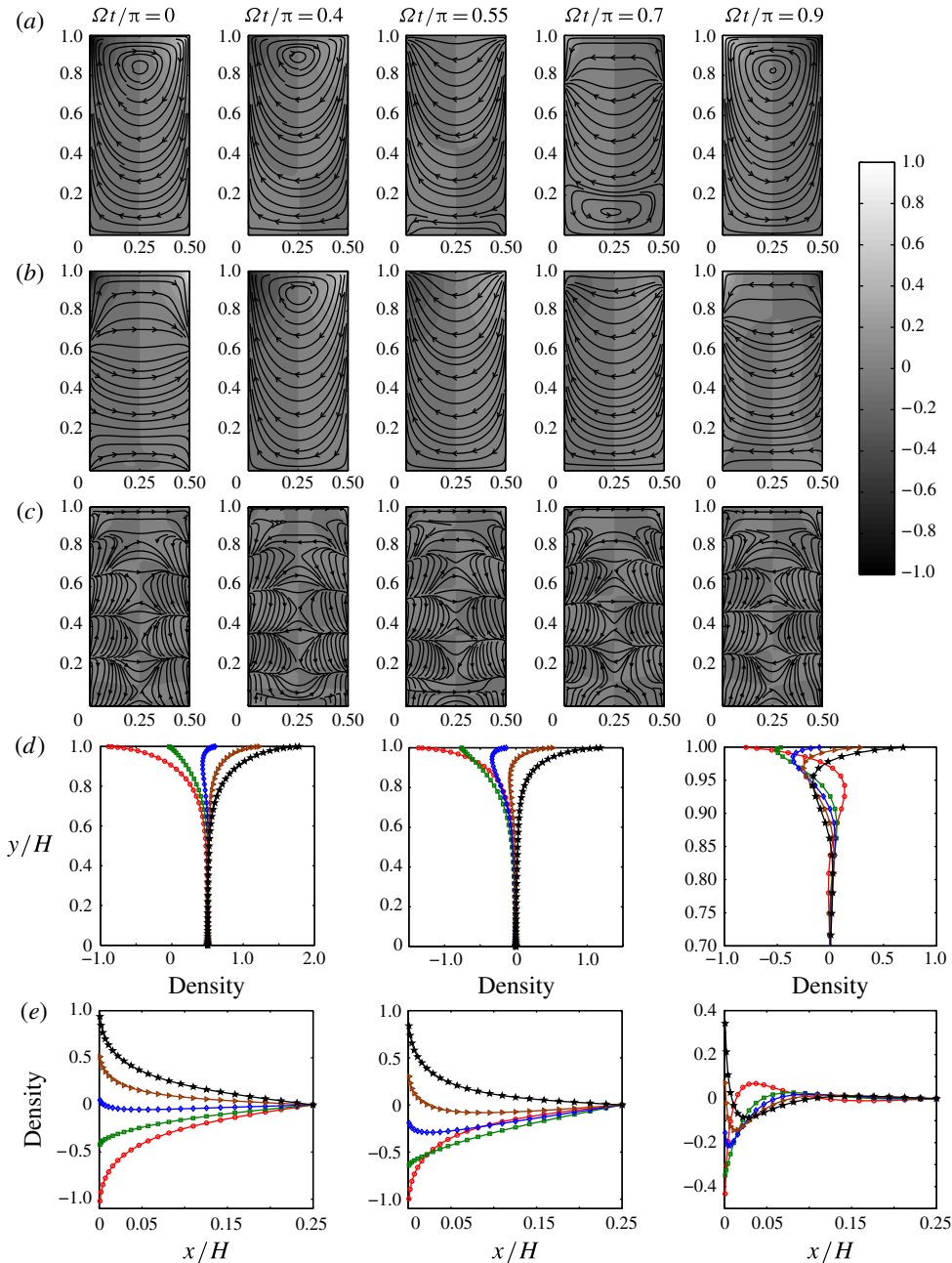


FIGURE 2. (Colour online) (a–c) Instantaneous density and streamline profiles inside the cavity for $A = 0.5$ and $Kn = 0.1$, during the first half-period of oscillation, for Strouhal numbers (a) 2, (b) 4, (c) 30. (d,e) Time evolution of vertical (d, $x = 0$) and horizontal (e, $y = H$) density variation for, from left to right, $St = 2, 4$ and 30. Circles, squares, diamonds, triangles, and stars correspond to times $\Omega t/\pi = 0, 0.4, 0.55, 0.7, 0.9$, respectively. Due to symmetry, density profiles at $0.5H \geq x > 0.25H$ are not shown in (e).

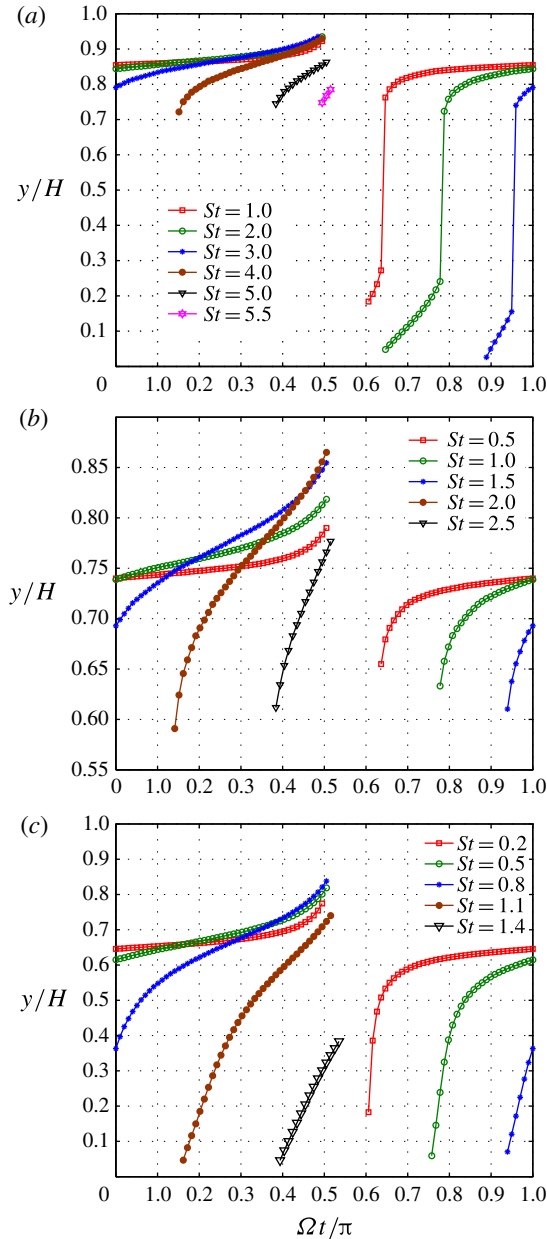


FIGURE 3. (Colour online) Variation with time of the location of the vortex centre during the first half-period of oscillation ($0 \leq \Omega t/\pi \leq 1$), for different values of St , and (a) $A = 0.5$, (b) $A = 1$, (c) $A = 2$. The Knudsen number is $Kn = 0.1$.

for the horizontal velocity at the oscillating lid (figure 4c), although its amplitude decreases when St increases, at high St it approaches $1/2$, except in small regions near the two vertical walls. The amplitude of the shear stress at the oscillating lid (figure 4d) increases with St in the central region of the oscillating lid and approaches a constant value $1/\sqrt{\pi}$ at high oscillation frequencies, as predicted by the analytical solution in (3.7).

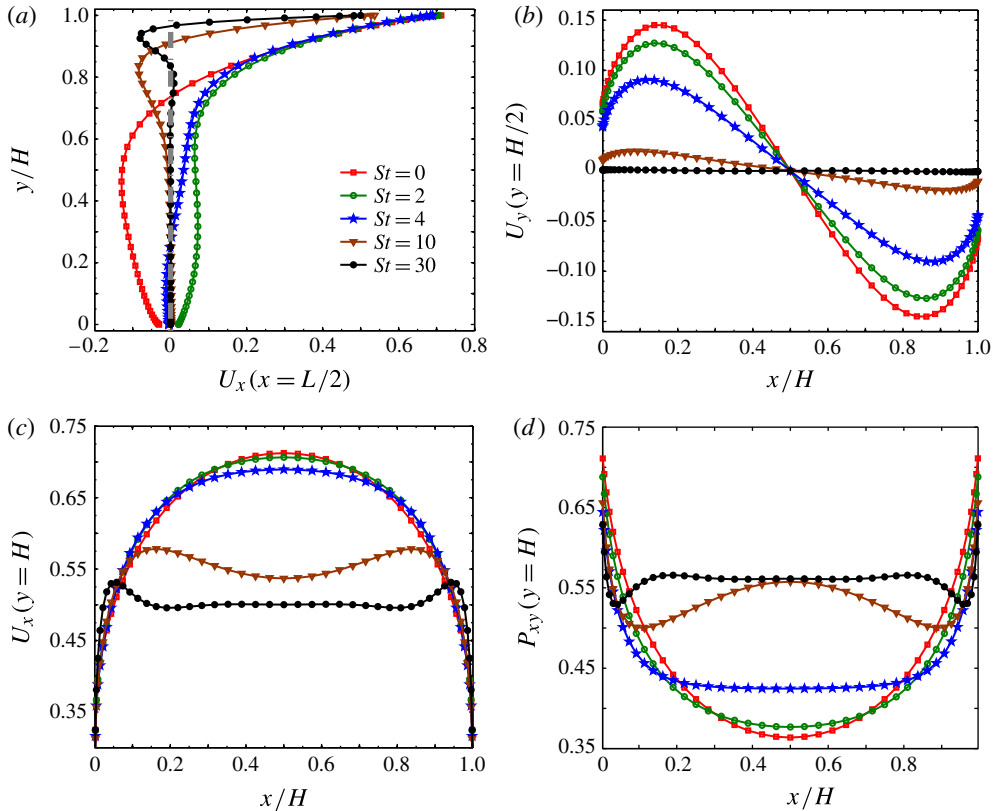


FIGURE 4. (Colour online) Amplitudes of (a) the central horizontal velocity $U_x(x=L/2)$, (b) central vertical velocity $U_y(y=H/2)$, (c) horizontal velocity $U_x(y=H)$ at the oscillating lid, and (d) shear stress $P_{xy}(y=H)$ at the oscillating lid, for different values of St , and with $A = 1$, $Kn = 0.1$.

Now we compare the average amplitudes of the horizontal velocity and shear stress along the oscillating lid with those in 1D oscillatory planar Couette flow. The results are shown in figure 5. For oscillating Couette flow, the gas velocity decreases monotonically as the Strouhal number increases, while the shear stress increases monotonically. However, for oscillatory lid-driven cavity flow, the average amplitudes of shear stress and horizontal velocity change non-monotonically. When $A = 0.5$, the average amplitude of shear stress first decreases and then increases towards the limiting value $1/\sqrt{\pi}$, and the average amplitude of horizontal velocity first increases and then decreases toward the limiting value $1/2$. However, for $A = 1$ and 2, the average amplitude of shear stress first increases, followed by a decrease, and then increases again monotonically towards the limiting value $1/\sqrt{\pi}$. The average amplitude of horizontal velocity varies in the opposite manner. Intuitively, because of the two vertical walls, the average horizontal velocity along the oscillating lid in a 2D oscillatory cavity flow should be smaller than that in a 1D oscillatory Couette flow, while the average amplitude of shear stress should be larger. From figure 5 we see that this is indeed the case when the oscillation frequency is small. However, at large St the average amplitude of shear stress in the 2D geometry is smaller than that of 1D oscillating Couette flow: for $A = 0.5$, the average shear stress in the 2D

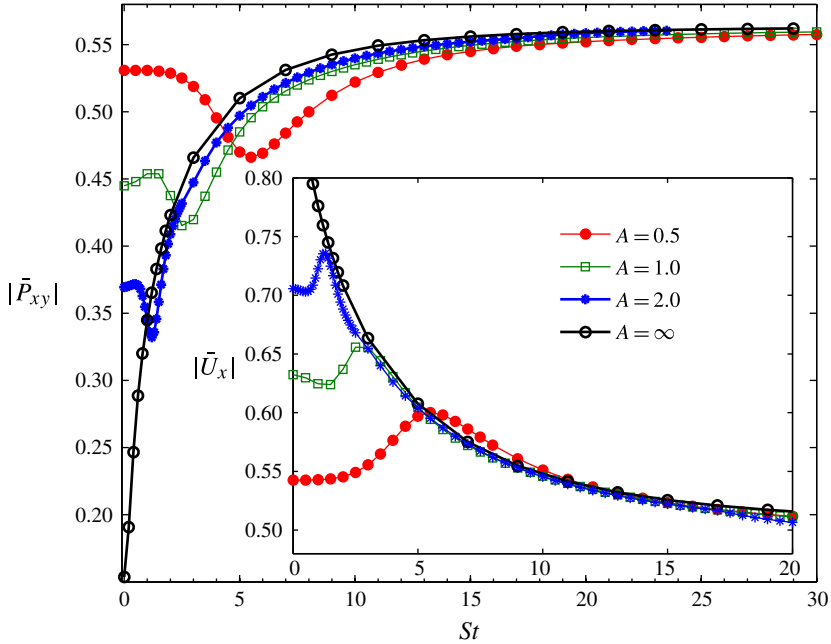


FIGURE 5. (Colour online) Variation of average amplitudes of the shear stress and horizontal velocity along the oscillating lid with St , for different values of the aspect ratio A and $Kn=0.1$. The $A=\infty$ results are for 1D oscillating Couette flow.

geometry is $\sim 10\%$ smaller than the 1D case at $St \approx 5.5$, while the average amplitude of the velocity in the 2D geometry is larger than the 1D case.

From a comparison between figures 3 and 5 we find that the minimum average amplitude of shear stress is reached when the vortex starts to disappear in the whole oscillation period. That is, when $A=0.5$ (or $A=1$ or 2), the vortex begins to disappear when $St > 5.5$ (or $St > 2.5$ or $St > 1.4$), which nearly coincides with values of St where the average amplitude of shear stress is a minimum. This minimum in shear stress is a result of the anti-resonance of the gas between two vertical walls, which we will discuss in § 3.4.

3.3. Transition and free-molecular flow regimes

We now consider the gas in the transition regime ($Kn=1$) and in the free-molecular flow regime ($Kn=10$). In both regimes, the left spatial half-region is divided into 26×51 non-uniform cells. For the discretization of molecular velocity space, we use $32 \times 32 \times 12$ grid points for $Kn=1$, and $48 \times 48 \times 12$ grid points for $Kn=10$.

The instantaneous density and streamline profiles are qualitatively the same as those for slip flows, and are omitted here. The amplitudes of the central horizontal and vertical velocities, and the horizontal velocity and the shear stress at the oscillating lid are shown in figure 6 for different Strouhal numbers when $Kn=1$. The results for $Kn=10$ are very similar to these for $Kn=1$, and are not shown here. As the Strouhal number increases, the central horizontal velocity varies within a small region near the lid (figure 6a), while the central vertical velocity gradually vanishes (figure 6b). Unlike in the slip flow regime, as St increases the horizontal velocity at the oscillating

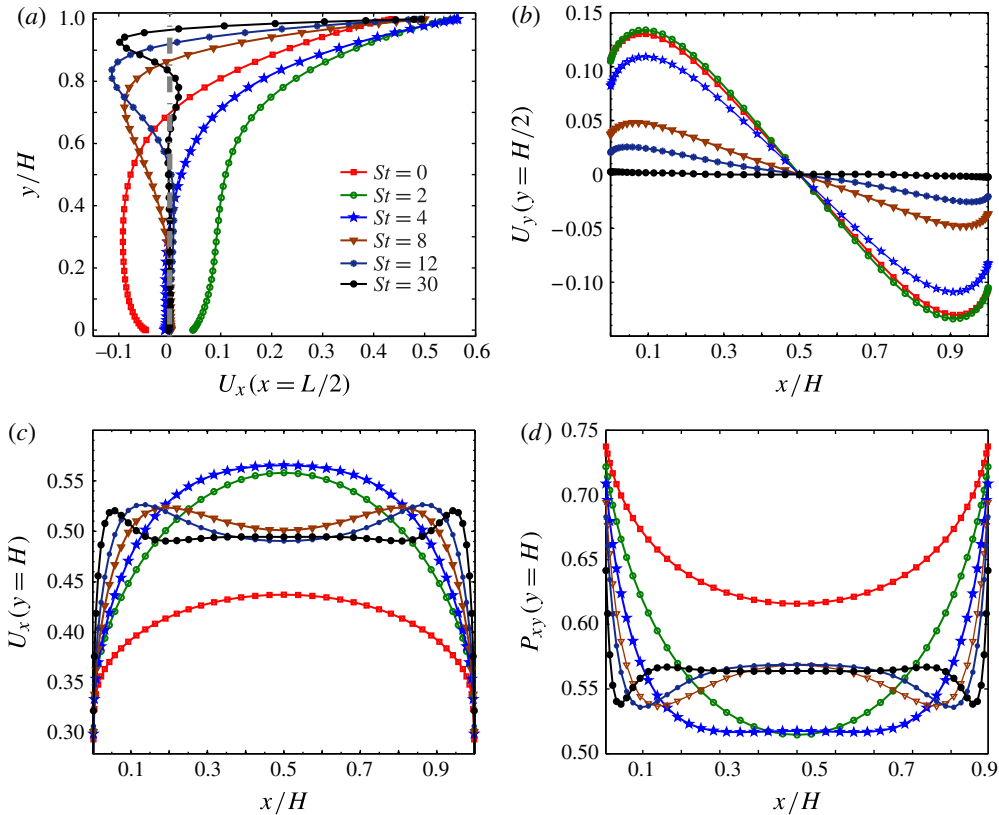


FIGURE 6. (Colour online) Amplitudes of (a) the central horizontal velocity $U_x(x=L/2)$, (b) central vertical velocity $U_y(y=H/2)$, (c) horizontal velocity $U_x(y=H)$ at the oscillating lid, and (d) shear stress $P_{xy}(y=H)$ at the oscillating lid, for different values of St , and with $A=1$, $Kn=1$.

lid first increases and then decreases to the limiting value $1/2$ (figure 6c), while the shear stress at the oscillating lid first decreases and then increases to the limiting value $1/\sqrt{\pi}$ (figure 6d).

The evolution of the average amplitude of shear stress at the oscillating lid with St for $Kn=1$ and 10 is shown in figure 7, which shows different behaviour from slip flows. In the transition and free-molecular flow regimes, the average amplitude of shear stress at small St is larger than the value at the high-frequency oscillation limit. For $Kn=1$, the average amplitude of shear stress at the lid (figure 7a) first decreases as the Strouhal number increases, and then increases toward the limiting value $1/\sqrt{\pi}$ (note that for $A=2$, at $St \approx 3$, a slight decrease in the shear stress occurs), while the average amplitude of horizontal velocity (figure 7b) varies in the opposite manner. For $Kn=10$, however, the average amplitude of shear stress and horizontal velocity oscillate about their limiting values as St increases (figure 7c,d). In both flow regimes, like in the slip flow regime, the average amplitude of shear stress in oscillatory cavity flow can be smaller than that in oscillatory Couette flow, over a certain frequency range. In oscillatory lid-driven cavity flow, we note that when $A=2$ the minimum average amplitudes of the shear stress are $\sim 23\%$ and 28% smaller than the maximum ones at $St=0$ when $Kn=1$ and 10 , respectively.

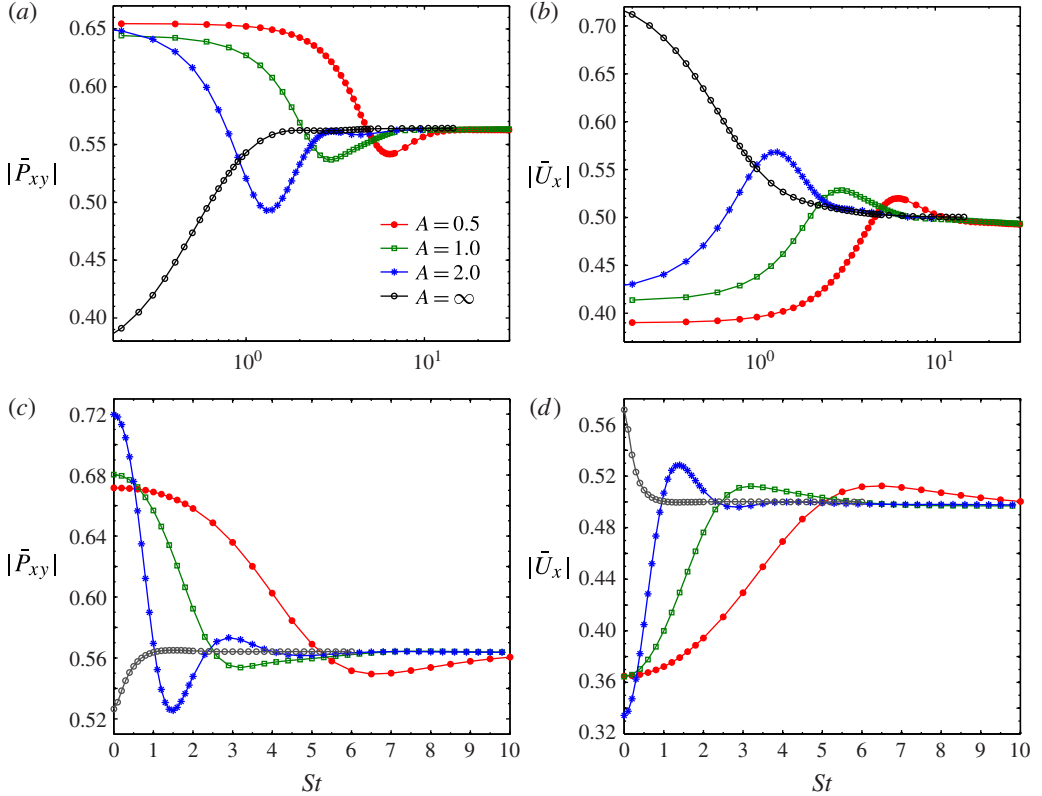


FIGURE 7. (Colour online) Variation of average amplitudes of the shear stress (a,c) and horizontal velocity (b,d) along the oscillating lid with St , for different values of the aspect ratio A , and for $Kn=1$ (a,b) and $Kn=10$ (c,d). The $A=\infty$ results are for 1D oscillating Couette flow.

3.4. Scaling law for anti-resonant frequency

From figures 5 and 7 we see that the Strouhal number at which the average amplitude of the shear stress at the lid is a minimum decreases as the aspect ratio of the cavity increases. Let us denote this the critical Strouhal number. Figure 8 displays a linear relation between the critical Strouhal number and inverse aspect ratio for $Kn=0.1$ and 1. The results for $Kn=10$ are not shown because they almost overlap those for $Kn=1$. This linear relation could help us choose the cavity aspect ratio that reduces the damping force that the gas exerts on the oscillating lid, for a given oscillation frequency.

The dip in the average amplitude of shear stress in figures 5 and 7 can be interpreted qualitatively as the gas anti-resonance between the two vertical walls. For simplicity, we consider the free-molecular flow. Using the method of characteristics, (3.1) can be rewritten as $iSt h + \mu \partial h / \partial s = 0$, where $\mu = \sqrt{v_x^2 + v_y^2}$ is the velocity and s is the coordinate along the characteristic line (Varoutis, Valougeorgis & Sharipov 2008). For the most probable velocity, the equation becomes $iSt h + \partial h / \partial s = 0$, which shows that the phase of the VDF remains unchanged after molecules have propagated a distance of $2\pi/St$. Now, let us consider molecules leaving the top lid with velocities nearly parallel to the top lid, hitting the right-hand vertical wall, then

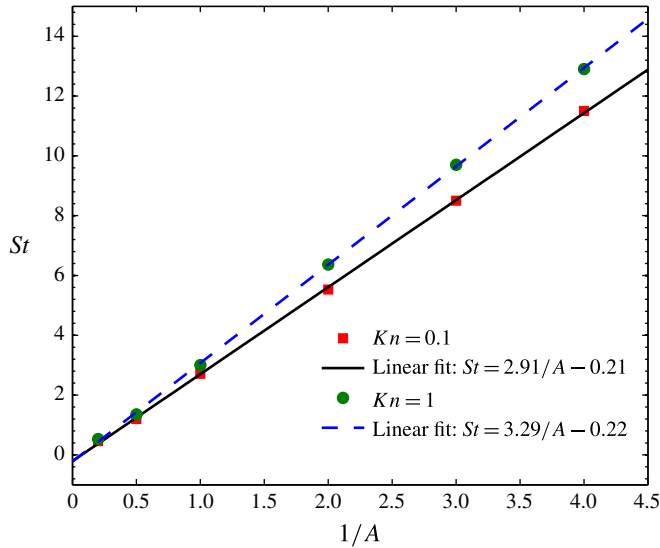


FIGURE 8. (Colour online) The critical Strouhal number (i.e. the St for which the average amplitude of the shear stress at the lid is minimum) as a linear function of the inverse aspect ratio $1/A$.

being reflected and hitting the left-hand vertical wall, and finally returning to the point from which they left. The normalized distance they have travelled is $\sim 2A$. If $A = \pi/St$, then molecules leaving and hitting the top lid have the same phase. Thus, the horizontal gas velocity at the oscillating lid is a maximum, and, since molecules leaving and approaching the top lid have opposite vertical velocities, the shear stress is a minimum. This theoretical prediction, i.e. that the anti-resonance Strouhal number is

$$St_a \approx \frac{\pi}{A}, \quad (3.8)$$

is in reasonable agreement with the numerical results shown in figure 8 for $Kn = 1$ and 10. For small Knudsen number, due to the frequent binary collisions, the anti-resonance Strouhal number is slightly less than π/A .

We note that a similar linear scaling law has been discovered by Desvilletes & Lorenzani (2012) for the propagation of sound waves between two planar plates. Their configuration is similar to that given in figure 1 if the top and bottom walls are removed and the left-hand wall oscillates in the x direction with frequency Ω . Their results showed that the normal pressure at the oscillating plate is a maximum when the resonant condition is achieved, that is, $St = 2\pi/A \times 0.48 \sim \pi/A$ (note that $A = 1$ in Desvilletes & Lorenzani 2012). This phenomenon can be interpreted in exactly the same way as we explained the minimum shear stress above. Consider molecules leaving the left-hand wall, being reflected at the right-hand wall, and returning to the left-hand wall: when $St = \pi/A$, molecules leaving and approaching the left-hand wall are in-phase. Hence the normal pressure is a maximum; however, the average amplitude of horizontal velocity is a minimum since the horizontal velocities are opposite.

The above analysis demonstrates that the resonance (anti-resonance) condition for the normal pressure in the 1D sound wave problem is the same as the anti-resonance

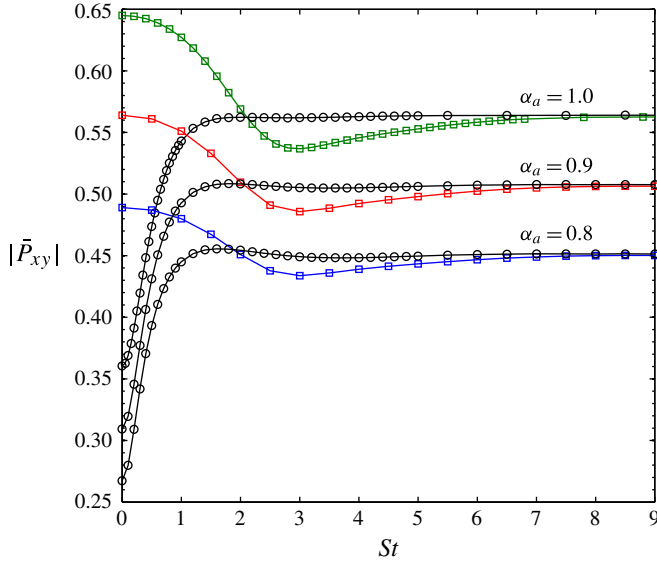


FIGURE 9. (Colour online) Variation of average amplitudes of shear stress at the oscillating lid with St , for $Kn=1$ and $A=1$ (squares), and different values of the surface accommodation coefficient α_a . The circles are the results for 1D oscillatory planar Couette flow.

(resonance) condition for the shear stress in 2D oscillatory cavity flow. In the 1D sound wave problem the anti-resonance is clearly seen when $St = \pi/2A$ (Desvillettes & Lorenzani 2012). However, the resonance in oscillatory cavity flow is only visible at small Kn , see figure 5 when $A=1$ and 2. That the resonance is relatively weaker in the 2D geometry may be because the kinetic energy input from the oscillating plate transfers vertically. For large Kn , it is more difficult for energy to be transferred from the oscillating lid to the bulk fluid, so the resonance is only observed at small Kn .

3.5. Influence of the boundary condition

We now study the influence of the boundary condition on the flow properties. We consider diffuse–specular wall boundary conditions, that is, an α_a proportion of the molecules hitting the wall are diffusively reflected, while the rest are specularly reflected, where $\alpha_a \in [0, 1]$ is the surface accommodation coefficient. So the boundary condition, for example, at the top lid, is

$$h(v_y < 0) = \alpha_a \left(2v_x + 2\sqrt{\pi} \int_{v_y > 0} v_y h d\mathbf{v} \right) f_{eq} + (1 - \alpha_a)h(-v_y). \quad (3.9)$$

Following the analytical calculations of § 3.1, it can be concluded that the average amplitudes of horizontal velocity and shear stress at the oscillating lid are $\bar{U}_x(y=H) = \alpha_a/2$ and $\bar{P}_{xy}(y=H) = \alpha_a/\sqrt{\pi}$. We would therefore expect that the surface accommodation coefficient affects the macroscopic flow quantities proportionately by a factor of $1 - \alpha_a$ relative to flow quantities calculated using the diffuse boundary condition. This is verified in the numerical simulations shown in figure 9. We also find that the surface accommodation coefficient does not change the anti-resonant frequency.

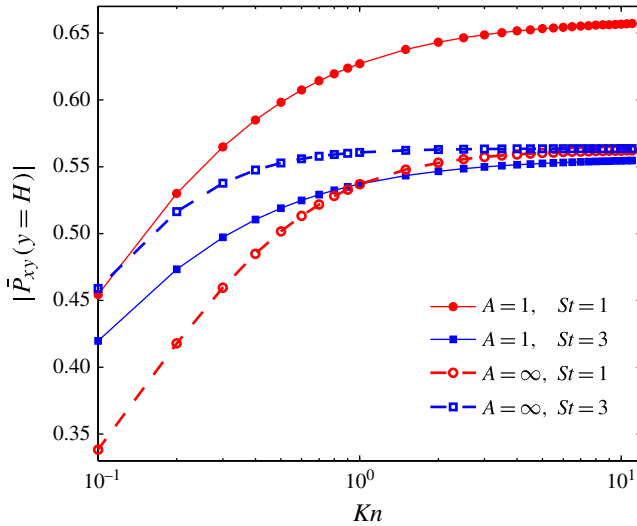


FIGURE 10. (Colour online) Variation of the average amplitude of the shear stress at the oscillating lid with the Knudsen number.

3.6. Variation of average amplitude of shear stress with Knudsen number

Finally, we show how the average amplitude of the shear stress at the oscillating lid varies with Kn , for a fixed oscillation frequency and cavity aspect ratio. The results are shown in figure 10 for a surface accommodation coefficient of 1. We see that for both oscillatory lid-driven cavity ($A = 1$) and Couette ($A = \infty$) flows, the average amplitude of shear stress increases monotonically until reaching some limiting value, which depends on the aspect ratio and the Strouhal number. At small oscillation frequencies, the damping in the cavity is always larger than the damping in the oscillatory Couette flow, while this situation is reversed near the anti-resonant oscillation frequency (i.e. at $St = 3$ for $A = 1$) over the whole range of Knudsen number.

4. Summary

The linearized Boltzmann equation has been applied to oscillatory lid-driven two-dimensional cavity flows of rarefied gases in the slip, transition and free-molecular flow regimes, over the whole range of oscillation frequency. The influence of the aspect ratio of the cavity on the damping force at the oscillating lid has been analysed in detail. We found that when the anti-resonance condition is satisfied, the damping force in the 2D cavity flow has a local minimum, which can be smaller even than the damping force in 1D oscillatory Couette flow. A linear scaling law between the anti-resonant frequency and the cavity aspect ratio has been established, and this could help in choosing the appropriate device geometry to reduce the damping force in MEMS technologies. The influence of a three-dimensional geometry on the damping is the subject of future research.

Acknowledgements

Y.Z. thanks the Royal Academy of Engineering (RAE) and the Leverhulme Trust for the award of a RAE/Leverhulme Senior Research Fellowship. This work is financially

supported by the UK's Engineering and Physical Sciences Research Council (EPSRC) under grants EP/I036117/1 and EP/I011927/1. The authors also thank the reviewers of this paper for their constructive suggestions.

REFERENCES

- BHATNAGAR, P. L., GROSS, E. P. & KROOK, M. 1954 A model for collision processes in gases. I. Small amplitude processes in charged and neutral one-component systems. *Phys. Rev.* **94**, 511–525.
- BIRD, G. A. 1994 *Molecular Gas Dynamics and the Direct Simulation of Gas Flow*. Oxford University Press.
- CERCIGNANI, C. 1990 *Mathematical Methods in Kinetic Theory*. Plenum.
- DESVILLETES, L. & LORENZANI, S. 2012 Sound wave resonance in micro-electro-mechanical systems devices vibrating at high frequencies according to the kinetic theory of gases. *Phys. Fluids* **24**, 092001.
- DOI, T. 2009 Numerical analysis of oscillatory Couette flow of a rarefied gas on the basis of the linearized Boltzmann equation. *Vacuum* **84**, 734–737.
- DUCK, P. W. 1982 Oscillatory flow inside a square cavity. *J. Fluid Mech.* **122**, 215–234.
- EMERSON, D. R., GU, X. J., STEFANOV, S. K., SUN, Y. H. & BARBER, R. W. 2007 Nonplanar oscillatory shear flow: from the continuum to the free-molecular regime. *Phys. Fluids* **19**, 107105.
- GOSPODINOV, P., ROUSSINOV, V. & STEFAN, S. 2012 Nonisothermal oscillatory cylindrical Couette gas–surface flow in the slip regime: a computational study. *Eur. J. Mech. (B/Fluids)* **33**, 14–24.
- GU, X. J. & EMERSON, D. R. 2011 Modeling oscillatory flows in the transition regime using a high-order moment method. *Microfluid Nanofluid* **10**, 389–401.
- HADJICONSTANTINO, N. G. 2002 Sound wave propagation in transition-regime micro- and nanochannels. *Phys. Fluids* **14**, 802–809.
- HOLWAY, L. H. 1966 New statistical models for kinetic theory: methods of construction. *Phys. Fluids* **9**, 1658–1673.
- KALEMPA, D. & SHARIPOV, F. 2009 Sound propagation through a rarefied gas confined between source and receptor at arbitrary Knudsen number and sound frequency. *Phys. Fluids* **21**, 103601.
- KALEMPA, D. & SHARIPOV, F. 2012 Sound propagation through a rarefied gas: influence of the gas–surface interaction. *Intl J. Heat Fluid Flow* **30**, 190–199.
- KARNIADAKIS, G., BESKOK, A. & ALURU, N. 2005 *Microflows and Nanoflows: Fundamentals and Simulation*. Springer.
- MENG, J. P. & ZHANG, Y. H. 2011 Accuracy analysis of high-order lattice Boltzmann models for rarefied gas flows. *J. Comput. Phys.* **230**, 835–849.
- NARIS, S. & VALOUGEORGIS, D. 2005 The driven cavity flow over the whole range of the Knudsen number. *Phys. Fluids* **17**, 097106.
- PARK, J. H., BAHUKUDUMBI, P. & BESKOK, A. 2004 Rarefaction effects on shear driven oscillatory gas flows: a direct simulation Monte Carlo study in the entire Knudsen regime. *Phys. Fluids* **16**, 317.
- SHAKHOV, E. M. 1968 Generalization of the Krook kinetic relaxation equation. *Fluid Dyn.* **3** (5), 95–96.
- SHARIPOV, F. & KALEMPA, D. 2008a Numerical modelling of the sound propagation through a rarefied gas in a semi-infinite space on the basis of linearized kinetic equation. *J. Acoust. Soc. Am.* **124** (4), 1993–2001.
- SHARIPOV, F. & KALEMPA, D. 2008b Oscillatory Couette flow at arbitrary oscillation frequency over the whole range of the Knudsen number. *Microfluid Nanofluid* **4**, 363–374.
- SHI, Y. & SADER, J. E. 2010 Lattice Boltzmann method for oscillatory Stokes flow with applications to micro- and nanodevices. *Phys. Rev.* **81**, 036706.
- STRUCHTRUP, H. 2005 *Macroscopic Transport Equations for Rarefied Gas Flows: Approximation Methods in Kinetic Theory*. Springer.

- STRUCHTRUP, H. 2011 Resonance in rarefied gases. *Contin. Mech. Thermodyn.* **34**, 361–376.
- TAHERI, P., RANA, A. S., TORRILHON, M. & STRUCHTRUP, H. 2009 Macroscopic description of steady and unsteady rarefaction effects in boundary value problems of gas dynamics. *Contin. Mech. Thermodyn.* **21**, 423–443.
- TANG, G. H., GU, X. J., BARBER, R. W., EMERSON, D. R. & ZHANG, Y. H. 2008 Lattice Boltzmann simulation of nonequilibrium effects in oscillatory gas flow. *Phys. Rev.* **78**, 026706.
- VAROUTIS, S., VALOUGEORGIS, D. & SHARIPOV, F. 2008 Application of the integro-moment method to steady-state two-dimensional rarefied gas flows subject to boundary induced discontinuities. *J. Comput. Phys.* **227**, 6272–6287.
- WU, L., REESE, J. M. & ZHANG, Y. H. 2014 Solving the Boltzmann equation by the fast spectral method: application to microflows. *J. Fluid Mech.* **746**, 53–84.
- YAP, Y. W. & SADER, J. E. 2012 High accuracy numerical solutions of the Boltzmann Bhatnagar–Gross–Krook equation for steady and oscillatory Couette flows. *Phys. Fluids* **24**, 032004.